Journal of *Marine Science and Engineering*

MDPI

Review

Hydro-Mechanical Interfacial Behavior of Offshore Foundations Under Uplift Loading

Maozhu Peng [1], Fuping Gao [2,*], Sen Mei [3] and Jun Cheng [4,5]

[1] Department of Civil and Environmental Engineering, The Hong Kong Polytechnic University, Hong Kong, China; maozhu.peng@polyu.edu.hk
[2] Institute for Ocean Engineering, Shenzhen International Graduate School, Tsinghua University, Shenzhen 518055, China
[3] School of Civil and Environmental Engineering, Nanyang Technological University, Singapore 639798, Singapore; sen.mei@ntu.edu.sg
[4] Institute of Mechanics, Chinese Academy of Sciences, Beijing 100190, China; chengjun@imech.ac.cn
[5] School of Engineering Science, University of Chinese Academy of Sciences, Beijing 100049, China
* Correspondence: gaofuping@sz.tsinghua.edu.cn

Abstract

Anchoring systems for deep-water floating structures must withstand complex, hydro-mechanical (H-M) coupled uplift forces throughout an operational life extending over decades, yet fundamental understanding of this complicated H-M behavior remains insufficient. This paper presents a comprehensive review of H-M coupled foundation–seabed interactions under uplift loading. Key experimental findings are synthesized to demonstrate that the fundamental distinction between uplift and compression lies in the foundation-soil interface. Unique interfacial uplift behaviors are highlighted, including the progressive formation of an interfacial gap and the evolution of transient suction within it. This water-filled gap enables sustained tensile contact stress post-detachment, transforming traditional soil-structure interaction to the more general "soil–interfacial fluid–structure" interaction framework. A 1D conceptual model, representing a mechanistic extension of Terzaghi's consolidation theory, is discussed to further elucidate these H-M mechanisms. For complex 3D numerical simulations, the limitations of traditional total-stress interface models are discussed, and specialized H-M thin-layer and zero-thickness interfaces designed for uplift modeling are critically examined regarding their advantages and limitations. The review concludes by outlining a roadmap for the next research frontier: high-fidelity treatments of sustained multidirectional cyclic loading, suction-induced liquefaction, and the long-term rheological evolution of the interface.

Keywords: offshore foundation uplift; soil-structure interaction; hydro-mechanical coupling; interfacial gap; numerical modeling

Check for updates

Academic Editor: Bang-Fuh Chen

Received: 27 May 2026
Revised: 27 June 2026
Accepted: 28 June 2026
Published: 1 July 2026

Copyright: © 2026 by the authors. Licensee MDPI, Basel, Switzerland. This article is an open access article distributed under the terms and conditions of the Creative Commons Attribution (CC BY) license.

1. Introduction

Uplift loading is omnipresent in offshore engineering, including the mooring of floating production platforms, sunken-vessel salvage, and the retrieval of jack-up spudcans and suction caissons. It also arises during the upheaval buckling of offshore pipelines. Recently, the rapid global deployment of offshore wind turbines has brought uplift problems to the forefront of foundation engineering. As of 2025, cumulative installed offshore wind capacity has reached 83 GW, projected to surge to 1950 GW by 2050 [1]. Meeting this demand requires a strategic transition toward deeper regions (depths > 60 m), where over 80% of

global offshore wind resources are located [2]. At such depths, traditional fixed-bottom turbines become economically infeasible [3], and floating turbines moored by anchoring systems emerge as the primary station-keeping solution, placing uplift resistance at the center of foundation design.

Despite its prevalence, uplift loading remains a persistent challenge for offshore geotechnical practice. For decades, foundation design has focused on compressive load-bearing capacity, with limited experience regarding sustained tensile uplift. Transitioning from compressive to uplift loading is not merely a reversal of force direction. Fundamentally distinct physical mechanisms have been identified experimentally [4–14]. These manifest as the gradual detachment of the foundation and the formation of an interfacial gap under uplift loading [4,12,15]. The mobilization and evolution of negative excess pore pressure (suction) within the gap [4,15] further complicate the behavior under uplift loading and distinguish it from its compressive counterpart. Together, these phenomena upscale the classical soil-structure interaction problem into the more complex framework of "soil–interfacial fluid–structure interaction" under uplift loading.

Conventional geotechnical methods typically neglect the development of the water-filled interfacial gap, assuming either fully bonded or zero-suction interface behaviors. This renders them mechanistically deficient in capturing transient hydro-mechanical (H-M) coupled behavior during uplift loading [16–18]. To avoid uncertainties resulting from these inadequate analysis approaches, current offshore practice usually relies on overly conservative assumptions that significantly drive up construction costs. This economic inefficiency remains a primary barrier to the global commercialization of floating offshore wind energy. A deep understanding of H-M interfacial behavior is therefore essential for facilitating the cost-effective design of floating mooring systems.

This article provides a narrative review of recent advancements in H-M coupled interfacial behavior during offshore foundation uplift, based on the authors' sustained research in this field. Relevant studies were identified iteratively and organized according to their contributions to experimental observations, analytical interpretation, and numerical modeling. As illustrated in Figure 1, the narrative progresses from fundamental experimental observations to an idealized 1D analytical framework and subsequent 3D numerical implementations. Rather than merely cataloging existing literature, this paper interprets the governing physical mechanisms through a consistent framework and demonstrates its significance in capturing foundation uplift performance. Existing interface models are critically examined, with their technical advantages and inherent limitations highlighted. The review concludes by identifying several frontiers requiring higher-fidelity H-M treatment. These include multidirectional cyclic loading, liquefaction, and the long-term evolution of the interface.

Existing reviews of offshore foundations [19,20] rarely focus on interfacial behavior and often oversimplify it, whereas reviews of interface models [18,21] seldom consider uplift loading. This review bridges this gap by synthesizing the hydro-mechanical interfacial behavior of offshore foundations under uplift loading. Throughout this review, compression is taken as positive. Suction and tensile contact stress are negative.

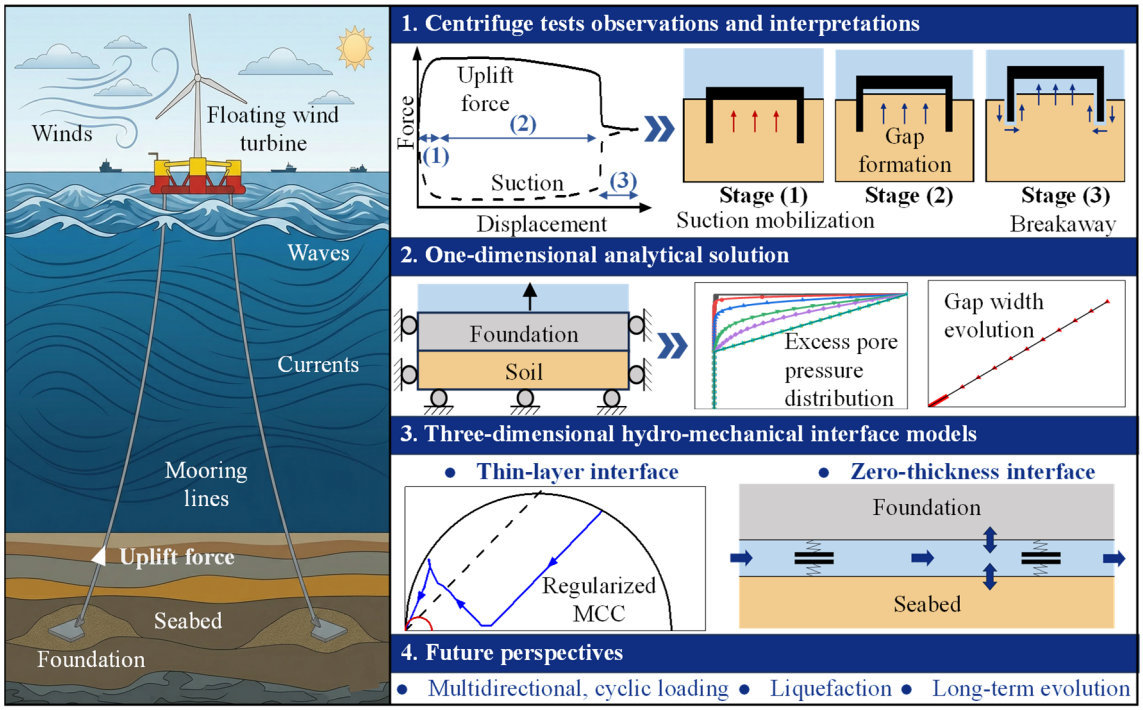


Figure 1. Overall layout of this paper.

2. Experimental Observations

The governing parameter for the H-M response of the foundation-soil interface is the dimensionless velocity (V) [22]:

$$V = \frac{vD}{c_v} \tag{1}$$

where v is the physical uplift velocity, D is the foundation diameter, and c_v is the coefficient of consolidation of soil. Equation (1) quantifies the competition between uplift and soil drainage rates, representing the ratio of the characteristic soil consolidation time to the foundation uplift time. As V increases, the soil transitions from a fully drained to a purely undrained state.

Early experimental investigations [5–7,23,24] on offshore foundation uplift primarily focused on the undrained regime, imposing a sufficiently fast uplift rate. These studies concluded that offshore foundations under undrained uplift loading exhibit a "reverse end-bearing" mechanism that mirrors the failure pattern of undrained compression. Consequently, the resulting uplift and compressive capacities are identical in magnitude. However, throughout the 20-year operational lifecycle of offshore structures, significant soil drainage inevitably occurs. This reality has necessitated a shift in research toward partially and fully drained conditions, where fundamentally distinct bearing mechanisms have been identified [4,9,11,25]. The following sections synthesize key experimental observations and their associated physical interpretations.

2.1. Centrifuge Test Results of Uplift at Varying Rates

Figure 2a presents typical centrifuge results for skirted foundation uplift across the full spectrum of drainage conditions, from fully drained to undrained states. Measurements were obtained for both the dimensionless uplift resistance (uplift force F normalized by foundation cross-sectional area A and soil strength at the skirt tip s_{u0}) and suction (negative excess pore pressure p normalized by s_{u0}) at the center of the foundation underside. At any given moment, the uplift force and the suction at the foundation underside are nearly equal in magnitude. Both exhibit a characteristic three-stage evolution (Figure 2b). Following

an initial rapid mobilization toward a peak value (Stage 1), both uplift resistance and suction enter a mild softening phase (Stage 2), ultimately culminating in the "breakaway" phenomenon (Stage 3). Complementary Particle Image Velocimetry (PIV) observations reveal that the breakaway stage is associated with a sudden increase in the interfacial gap opening width, as shown in Figure 3. The mechanisms underlying the three stages and their transitions are discussed in Section 2.2. Numerical approaches to reproduce the three stages will be discussed in Section 4.

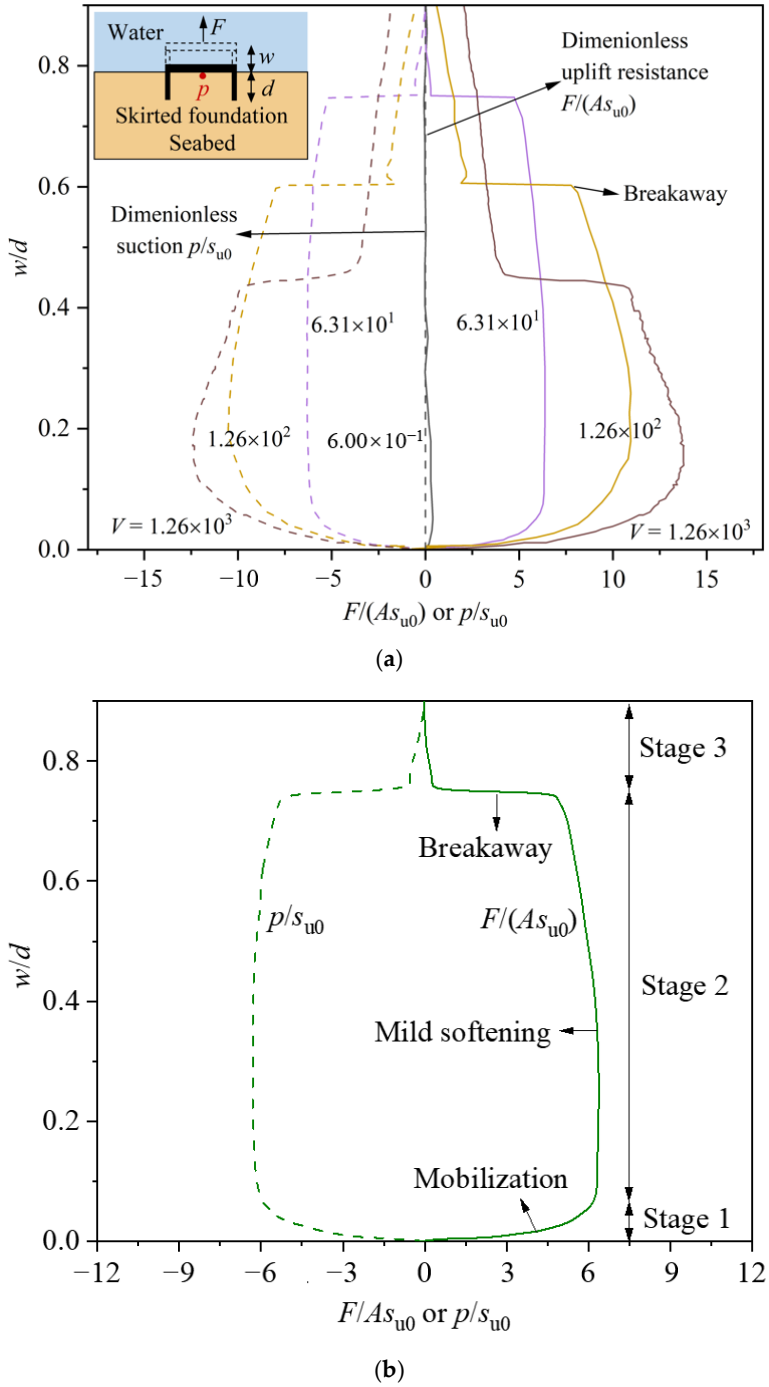


Figure 2. Centrifuge results of skirted foundation uplift at various rates (adapted from Li [4] and Peng et al. [15]): (**a**) Evolution of normalized uplift force $F/(As_{u0})$ and excess pore pressure p/s_{u0} against dimensionless foundation uplift distance w/d; (**b**) illustration of the three stages.

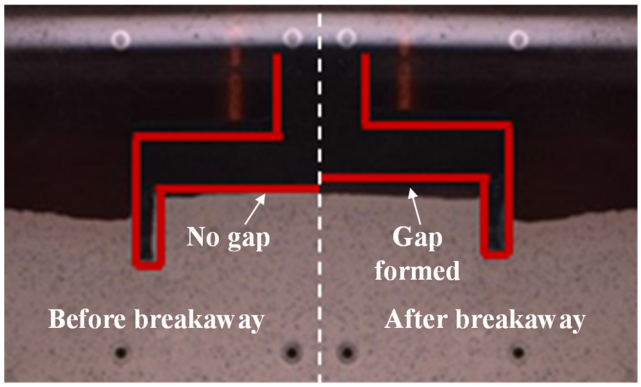


Figure 3. Experimentally observed gap opening width before and after breakaway (adapted from Peng et al. [15]).

Figure 2 also reveals the pronounced rate-dependency of offshore foundation uplift. Both the uplift resistance and the suction decrease consistently as the uplift velocity is reduced. This is directly linked to earlier breakaway timing and the increased opening width of the interfacial gap. The latter is reflected in the PIV results in Figure 4, where the vertical displacement of the internal soil plug is reduced at lower uplift rates. These findings were recently corroborated by the centrifuge investigations of Mei et al. [11,25], which further identify that skirt length critically influences the onset of breakaway, with shorter skirts exhibiting an earlier breakaway.

2.2. Interpretation Based on Experimental Observations

Based on the experimental observations presented above, this section interprets the H-M mechanisms governing the three-stage uplift response. Central to interpreting the above observations is characterizing the physical state of the interfacial gap that develops between the foundation base and the seabed. Although direct measurement of the gap's composition is infeasible during centrifuge testing, it can be deduced that the gap does not exist in a vacuum. Otherwise, the extreme suction associated with a vacuum would trigger immediate plastic failure of the underlying soil, forcing an upward soil flow to fill the void. Consequently, the gap must be occupied by water, which infiltrates the interface through flow. This establishes a fundamental governing principle: the rate of change in volume (opening rate) of the interfacial gap must equal the net fluid influx (assuming water is incompressible). This mass conservation requirement is the key to interpreting the following three-stage evolution (see Figure 2).

- Stage 1. At the onset of uplift loading, an uplift force is applied and causes the water within the incipient interface to undergo "stretching". This forces the fluid pressure to drop below the initial hydrostatic value. The resulting pressure deficit, or suction, alleviates the vertical confining stress on the underlying soil and induces a trend of upward deformation. This process activates the soil's shear strength, resulting in a rapid increase in uplift resistance.
- Stage 2. The suction generated at the interface establishes a hydraulic gradient within the seabed, driving ambient pore water to infiltrate the gap. This influx attenuates the mechanical stretching of the interfacial fluid, allowing the suction to dissipate toward a hydrostatic state and leading to the softening of the uplift resistance. Concurrently, the accumulation of pore water at the interface results in a progressive expansion of the water-filled gap. The expansion rate is governed by the pore water seepage velocity, as defined by Darcy's law $\mathbf{v}_w = (K/\gamma_w)\nabla p$, where $\mathbf{v}_w$ is the pore water seepage velocity (water velocity relative to soil skeleton), K is the soil permeability, γ_w is the water unit weight, p is the excess pore water pressure, and ∇ represents the gradient operator.

- Stage 3. As the foundation skirt approaches the mudline, preferential flow paths may develop along the skirt–soil interface. These allow seawater to short-circuit the soil matrix and directly flood the gap. This sudden influx results in an almost instantaneous loss of suction and a rapid expansion of the interfacial gap, culminating in the breakaway.

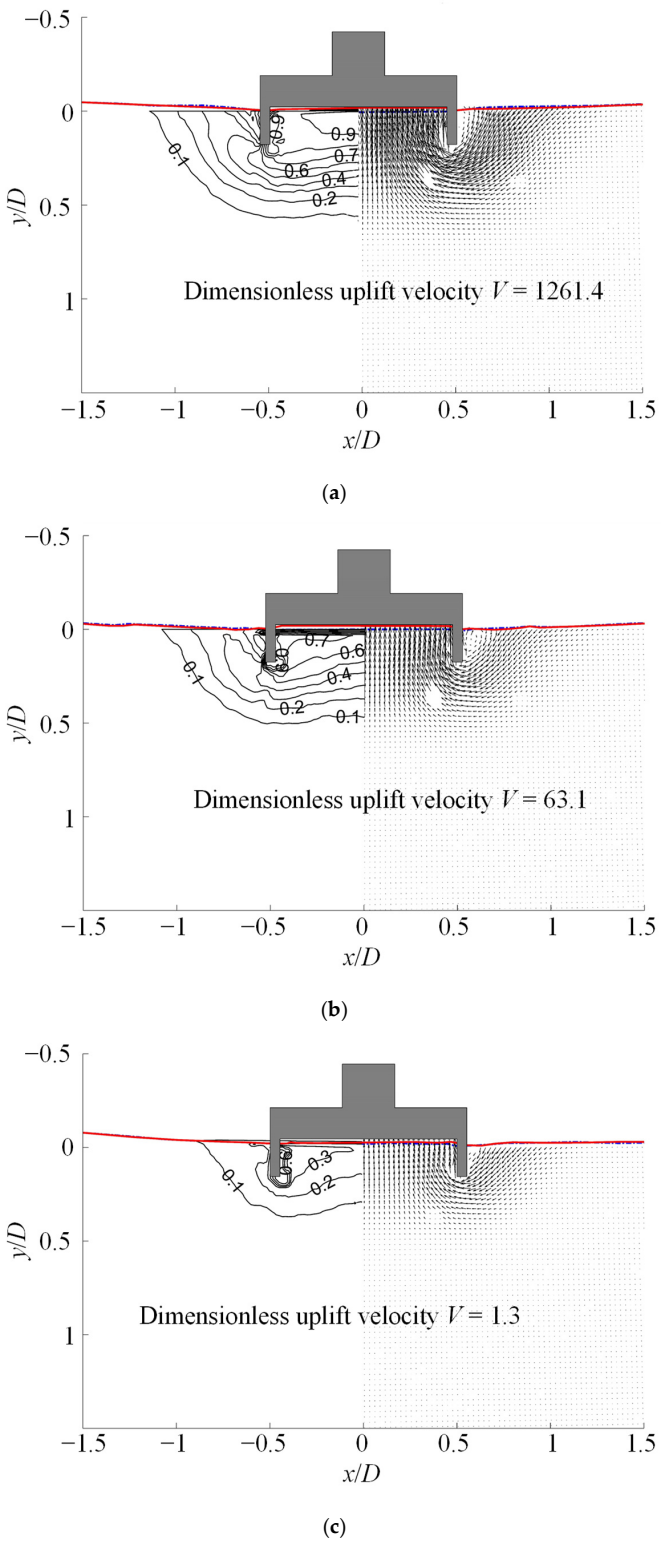


Figure 4. PIV observations on the skirted foundation uplift behavior at varying dimensionless uplift rate V (adapted from Peng et al. [15]): (**a**) V = 1261.4; (**b**) V = 63.1; (**c**) V = 1.3.

The above mechanism implies that the characteristics of these three stages are fundamentally dictated by the competition between the uplift rate and the seepage velocity. Under near-drained conditions, where the uplift rate is significantly lower than the seepage rate, pore water infiltrates the interface rapidly enough (relative to the uplift process) to equilibrate the suction. This results in a fully open gap and negligible uplift resistance. In contrast, at high uplift velocities, pore water lacks the necessary time to infiltrate the interface, causing it to remain fully closed until breakaway. In this undrained limit, the upward deformation of the soil plug inside the foundation fully mobilizes the soil's shear strength, thereby maximizing the system's uplift resistance.

It is worth noting that if the gap water pressure falls below the local vapor pressure, cavitation may occur. In this process, the gap water undergoes a phase change into vapor, meaning the gap opening rate is no longer solely a function of mass transport, as phase change also induces volumetric change. The following discussion primarily focuses on conditions where the gap water remains in a liquid state. The treatment of cavitation is briefly discussed in Section 4.2.3.

3. One-Dimensional (1D) Analytical Solution of H-M Behavior Under Uplift Loading

The H-M mechanism identified above facilitates the formulation of a 1D conceptual model (Figure 5), which represents an inverse analog to classical Terzaghi 1D consolidation theory. This model consists of two vertically aligned, saturated linear elastic porous media, representing the foundation (upper domain) and the soil (lower domain). The physical properties of these domains are characterized by their respective Young's moduli E_1 and E_2; Poisson's ratio $\nu_1 = \nu_2 = 0$; permeability K_1 and K_2; and height $h_1 = h_2 = 1$ m.

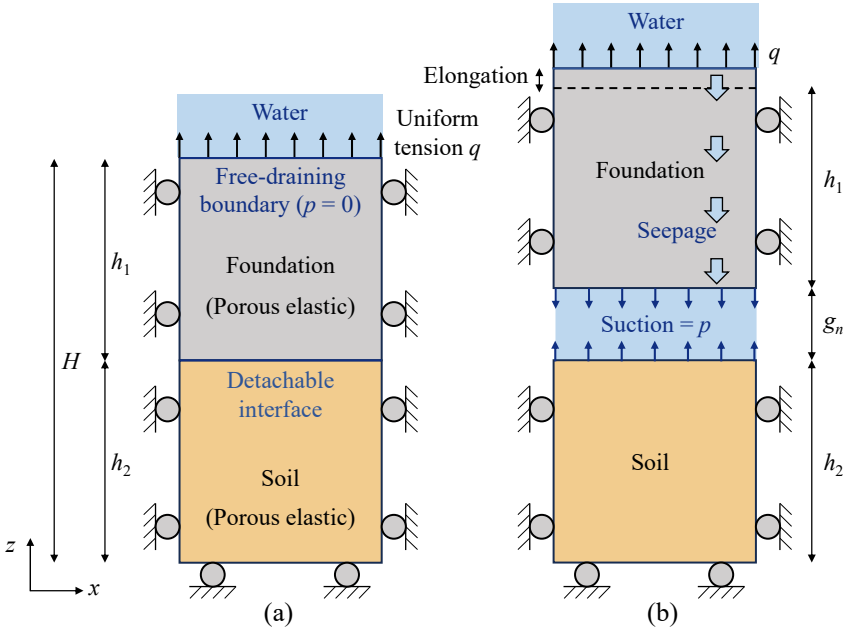


Figure 5. Conceptual illustration for 1D uplift loading of two saturated linear elastic bodies: (**a**) Initial configuration; (**b**) Deformed configuration.

All lateral surfaces are constrained against normal displacement. The top surface of the foundation is a free-draining boundary maintained at zero hydrostatic water pressure. All other external boundaries are assumed to be perfectly impermeable.

At time $t = 0$, a uniform tension q is applied to the top surface of the foundation. Under a quasi-static assumption, Peng et al. [26] derived analytical solutions for the spatial and temporal evolution of the excess pore water pressure. For the soil:

$$\frac{p(z,t)}{q} = 1 \qquad 0 \le z \le h_2 \tag{2}$$

For the foundation:

$$\frac{p(z,t)}{q} = 1 - \frac{z-h_2}{h_1} - \frac{2}{\pi}\sum_{n=1}^{\infty}\frac{(-1)^n}{n}\sin\left(n\pi\frac{z-h_2}{h_1}\right)\exp\left(-n^2\pi^2\frac{E_1K_1t}{\gamma_w h_1^2}\right) \quad h_2 \le z \le H \tag{3}$$

where $H = h_1 + h_2$ is the total height of the system, and n is the summation index. Equation (3) can be further combined with Darcy's law to calculate the opening rate of the interfacial gap:

$$\dot{g}_n = \frac{K_1}{\gamma_w}\frac{\partial p}{\partial z}\bigg|_{z=h_2} = -\frac{K_1 q}{h_1\gamma_w}\left[1 + 2\sum_{n=1}^{\infty}(-1)^n\exp\left(-n^2\pi^2\frac{E_1K_1t}{\gamma_w h_1^2}\right)\right] \tag{4}$$

where g_n is the gap opening width between the two objects, and the superposed dot denotes differentiation with respect to time. Integrating Equation (4) over time and applying the initial condition $g_n\,(t = 0) = 0$, the temporal evolution of the gap width can then be obtained.

Although the analytical solution elucidates the fundamental H-M mechanisms, its quantitative applicability is constrained by several simplifying assumptions. The one-dimensional formulation cannot represent lateral deformation, multidirectional seepage, or spatial variations in interfacial gap opening and suction. Furthermore, the foundation and soil are idealized as linear elastic porous media; consequently, soil yielding, stress-dependent stiffness, and irreversible deformation are excluded. The assumption of constant permeability also precludes changes associated with variations in stress and void ratio. Accordingly, the analytical solution should be regarded primarily as a conceptual framework for interpreting H-M interfacial behavior and as a benchmark for numerical formulations, rather than as a direct predictive model for offshore foundations.

4. Numerical Modeling of 3D H-M Uplift Problems

For general 3D uplift problems, deriving closed-form analytical solutions is unattainable, and only numerical solutions are achievable. Numerical modeling of soil-structure interaction relies on interface models. Conventional soil-structure interaction modeling typically employs interface formulations within a total stress framework, focusing on the constitutive relations between the interface displacements and the resulting contact stress. A comprehensive review of existing interface models is presented in Zhang & Zhang [18].

By neglecting the role of interfacial fluids, these models become fundamentally ill-suited for capturing the transient H-M processes inherent in offshore foundations under uplift loading. Current numerical practice predominantly relies on two simplified extremes [27–33]: (i) an "immediate-breakaway" interface, which assumes an instantaneous loss of contact stress upon detachment, and (ii) a "no-breakaway" interface, which artificially prohibits separation by allowing unrealistic tensile stresses to develop. Neither approach reflects the H-M coupled reality of offshore foundations under uplift loading, where tensile contact stress, manifested as transient suction, can persist after the foundation and soil have separated and can vary in real time. Accurately simulating this behavior necessitates specialized H-M interface models. These are generally categorized into two classes: thin-layer and zero-thickness interfaces.

4.1. H-M Thin-Layer Interface

4.1.1. Poroelastic Thin-Layer Interface

The thin-layer interface approach characterizes the foundation-soil contact as a thin continuum layer [34–38]. H-M coupling is enabled by combining the interface constitutive model with Biot's consolidation theory [39]. H-M thin-layer models originated from compressive loading conditions, aiming to simulate the deformation and drainage of soft infill within rock joints under squeezing. A fundamental prerequisite for these models is that the normal stiffness must increase progressively as the interface is compressed to preclude foundation penetration into the soil. A straightforward constitutive model satisfying this condition is poroelasticity: $e = e_0 - \kappa \ln p'$, where e is the void ratio of the interface continuum; $p' = (\sigma'_{xx} + \sigma'_{yy} + \sigma'_{zz})/3$ is the mean effective stress, κ is the bulk modulus, and e_0 is the void ratio at $p' = 1$. In this formulation, the stiffness increases exponentially as the interface is compressed (e decreases), preventing interpenetration.

Transitioning to uplift scenarios imposes an additional constraint: the effective normal contact stress must vanish and remain at zero upon detachment. This requirement is a direct consequence of the observation in Figure 2 that tensile contact stress at the interface is derived solely from fluid suction, and the soil skeleton cannot mobilize tensile effective stress. The poroelastic H-M thin-layer interface fails to satisfy this requirement. The logarithmic term ($\ln p'$) poses a mathematical singularity as p' approaches zero. This can be mitigated by introducing a small tolerance tol, such that $p' = \max(p', tol)$.

The above poroelastic thin-layer interface was pioneered by Mana et al. [36] for investigating seepage under a skirted foundation and subsequently refined within large-deformation finite element frameworks to simulate plate anchors under uplift loading [35]. While its implementation is straightforward, the approach suffers from a significant physical limitation: the interface can never achieve a fully closed state.

4.1.2. Critical State Elastoplastic Thin-Layer Interface

To achieve a mechanistically rigorous representation of the fully closed state, a more robust strategy [40–44] involves employing an elastoplastic constitutive model based on the Critical State Soil Mechanics (CSSM) framework [45,46] as the interface material. This allows the thin-layer interface to behave as a continuum soil under compression, representing the closed state. Under tensile loading, the softening mechanism inherent in CSSM allows the yield surface to progressively contract toward the origin of the effective stress space ($\boldsymbol{\sigma}' = 0$). At this limit, all effective mechanical stresses within the interface vanish, and the total uplift resistance is provided exclusively by fluid suction, accurately capturing the physics corresponding to the detached state.

However, this detached state represents a numerical singularity within traditional CSSM formulations and is associated with numerical instability. Utilizing the Modified Cam–Clay (MCC) model as a baseline, Peng et al. [17] proposed an effective regularization strategy by introducing a "no-softening surface" (Figure 6). This constrains the effective interface stresses to a negligible level while preventing the yield surface from collapsing into a single point. The efficacy of this approach has been validated across diverse loading scenarios [17,47]. As illustrated in Figure 7, the proposed model outperforms the standard MCC model in commercial FE software Abaqus under partially and fully drained conditions, where the Abaqus built-in MCC suffers from premature failure.

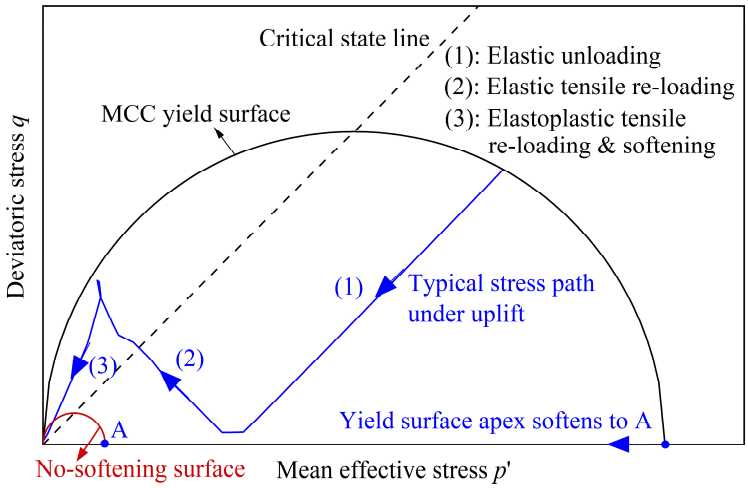


Figure 6. Illustration of the introduction of a no-softening surface into the MCC model (adapted from Peng et al. [17]).

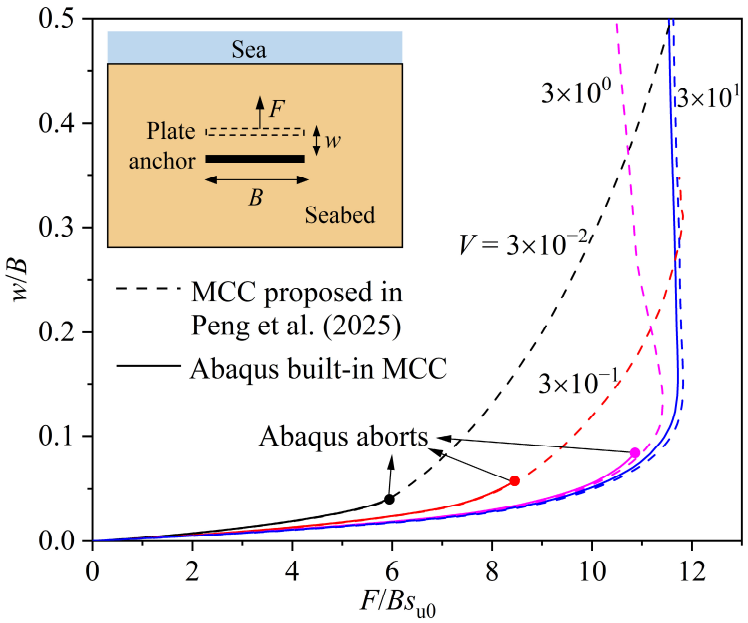


Figure 7. Performance of the proposed MCC thin-layer interface model and comparison with the Abaqus built-in MCC model (adapted from Peng et al. [17]).

The proposed MCC interface allows visualization of the foundation–seabed detachment process. As shown in Figure 8, the model captures distinct interfacial gap opening rates as a function of the dimensionless uplift velocity (V): (i) a fully closed interface during rapid uplift loading (V = 300), where the soil elements beneath the foundation do not elongate and the underlying soil is fully drawn up by high suction; (ii) a partially open interface at intermediate uplift velocities (V = 3), characterized by moderate vertical elongation of the interface elements; and (iii) a fully open interface at low uplift velocities (V = 0.03), where the soil remains stationary as the foundation detaches. These numerical results are qualitatively consistent with the PIV observations described in Figure 4. Notably, the standard MCC implementation in Abaqus is incapable of capturing the detached states shown in Figure 8b,c due to the aforementioned numerical singularity.

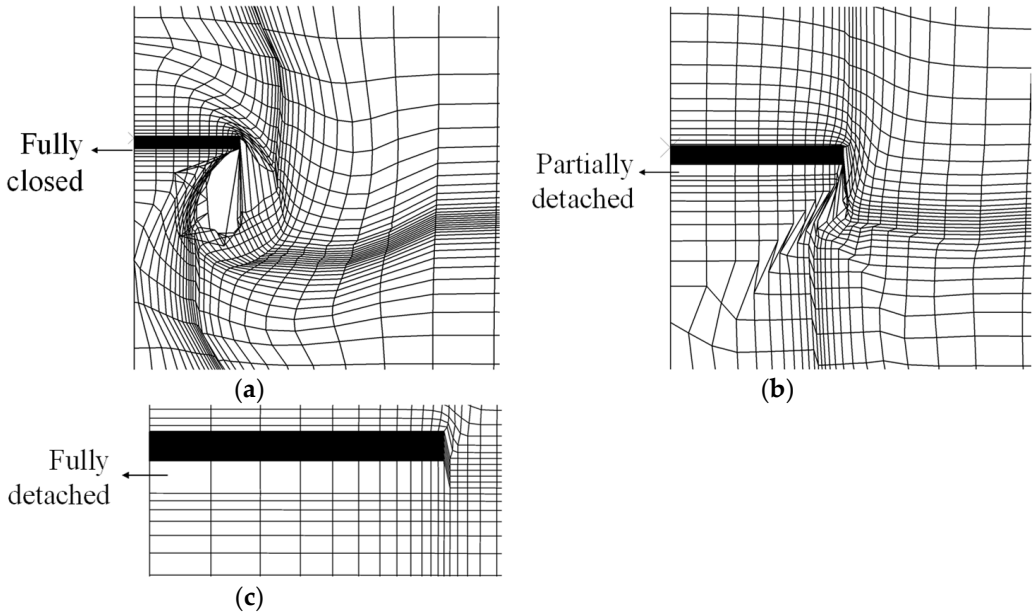


Figure 8. Performance of the proposed MCC thin-layer interface in simulating foundation-soil detachment: (**a**) Fully closed interface at fast uplift velocity (V = 300); (**b**) Partially open interface at intermediate uplift velocity (V = 3); (**c**) Fully open interface at slow uplift velocity (V = 0.03).

Despite these improvements, two primary limitations of the thin-layer MCC interface approach persist. First, the framework lacks an explicit kinematic mechanism for measuring the physical gap opening width. Instead, separation is represented approximately through the vertical elongation of the continuum elements. Second, while the method successfully reproduces rate-dependent resistance and the transient softening observed in, for example, Figure 7 (V = 3), it remains mechanistically incapable of capturing the abrupt breakaway behavior characteristic of Stage 3.

Furthermore, parameter calibration of the MCC model requires extra effort. The conventional MCC parameters can be obtained from standard oedometer, triaxial, and permeability tests. The size of the no-softening surface is the only additional parameter and can be selected through sensitivity analysis to ensure that it is sufficiently small not to affect the numerical results. However, parameters derived from element tests may not accurately reproduce soil behavior in boundary-value problems. For practical applications, they may therefore require calibration against field observations through iterative back-analysis. Recent advances in intelligent parameter identification [48–50] provide a promising means of automating and accelerating this process.

4.2. H-M Zero-Thickness Interface

4.2.1. General Formulation

Diverging from the continuum-based thin-layer approach, the zero-thickness interface [16,51–55] models the foundation-soil contact as a physical discontinuity (Figure 9). Within this framework, the effective normal contact stress (σ'_n) is determined by the normal gap opening width (g_n) through $\sigma'_n = -k_n g_n$, where k_n represents the normal stiffness of the interface, with $k_n \to \infty$ when the gap is closed ($g_n \leq 0$) and $k_n = 0$ otherwise.

Similarly, the tangential contact stress (σ_t) is calculated using the tangential relative displacement of the interface (g_t) according to the Coulomb friction law: $\sigma_t = k_t g_t$ if $k_t g_t < v\sigma'_n$ and $\sigma_t = v\sigma'_n$ otherwise, where $k_t \to \infty$ is the interface tangential stiffness, and v is the friction coefficient at the interface.

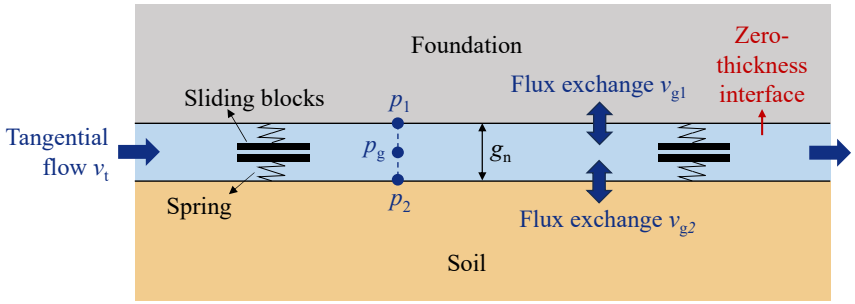


Figure 9. Illustration of the zero-thickness interface model (adapted from Peng et al. [16]).

Hydraulically, the zero-thickness interface assumes the fluid pressure within the gap (p_g) is uniform across its thickness but remains distinct from the pore pressures (p_1 and p_2) at the adjacent foundation and soil boundaries. The rate of fluid exchange between the interfacial gap and the foundation or soil is described by a leak-off model [16,52,53]:

$$v_{g1} = c_1(p_g - p_1); \quad v_{g2} = c_2(p_g - p_2) \tag{5}$$

where v_{g1} and v_{g2} are the fluid exchange rates between the interfacial gap and foundation and soil, respectively; and c_1 and c_2 are leak-off coefficients.

In addition to fluid flow in the normal direction, the interface accommodates tangential fluid transport along the gap. Two distinct flow patterns are considered [16]. Poiseuille flow (Figure 10a) is suitable for open gaps where the fluid velocity follows a parabolic profile, resulting in a volumetric flux (Q_t) governed by the cubic law [56]:

$$Q_t = \frac{g_n^3}{12\mu}\nabla p_g \tag{6}$$

where μ is the dynamic viscosity of water.

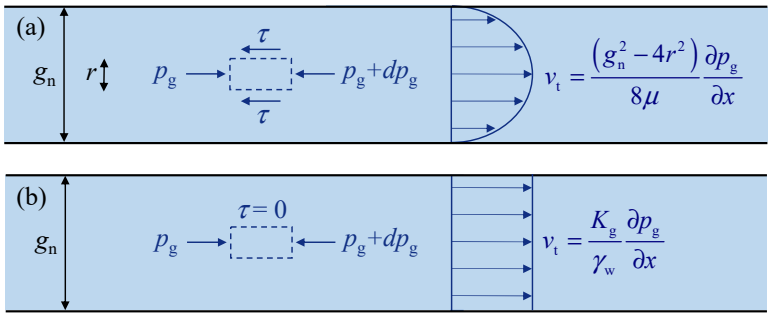


Figure 10. Schematic illustration of two types of tangential flow: (**a**) Poiseuille flow; (**b**) Darcy flow.

Conversely, Darcy flow (Figure 10b) is more appropriate for quasi-closed interfaces where fluid transport resembles flow through a porous medium, with the tangential flux expressed as:

$$Q_t = g_n\frac{K_g}{\gamma_w}\nabla p_g \tag{7}$$

where K_g is the tangential permeability of the interface.

The H-M coupling within the zero-thickness interface is enforced through the principle of mass conservation of the interfacial fluid. Assuming incompressible water, the governing equation stipulates that the gap opening rate is determined by the net normal fluid influx from the adjacent porous media and the divergence of the tangential flow:

$$-\nabla Q_t + v_{g1} + v_{g2} + \dot{g}_n = 0 \quad (8)$$

Derived from the Goodman element [57], early zero-thickness interface models [58] were purely mechanical and developed primarily for compressive loading. Segura & Carol [53,54], among others, pioneered H-M zero-thickness interface formulations, initially to describe fluid flow within rock joints. Cerfontaine et al. [52] appear to be among the first to apply the H-M zero-thickness interface to simulate offshore foundation uplift. Lai et al. [59] subsequently fine-tuned an H-M cohesive element to investigate the drainage-dependent uplift response of suction caissons. The cohesive element may be regarded as a specialized H-M zero-thickness element incorporating sophisticated mechanical damage formulations originally developed for describing cracking of rock joints. Because these additional mechanical features are not essential for foundation uplift simulation and may unintentionally affect the predicted response, application of the H-M cohesive element approach is less straightforward. In the above studies, tangential flow was represented solely by Poiseuille flow (Figure 10a). Moreover, seabed pore water was assumed to be the only source of fluid entering the interface, with exchange between the gap water and external seawater neglected. Building on these formulations, Peng et al. [16] introduced Darcy-type tangential flow (Figure 10b) and enabled the gap water–seawater exchange. These extensions allowed key features of the experimentally observed force–displacement curves (Figure 2) to be reproduced, as discussed below. Mei et al. [60] subsequently adopted a similar approach to simulate centrifuge tests and obtained good agreement.

Peng et al. [16] systematically evaluated the performance of this H-M zero-thickness interface by simulating the uplift loading of a surface foundation across a range of velocities. As presented in Figure 11a, numerical results utilizing the Poiseuille tangential flow model effectively replicate the qualitative rate-dependency and the abrupt breakaway phenomenon observed experimentally in Figure 2. The evolution of the gap opening width at the foundation center is depicted in Figure 11b. Under low uplift velocities, the gap begins to expand almost immediately upon the initiation of loading. Conversely, under high uplift velocities, the interface remains effectively sealed during the initial stages before undergoing a sudden breakaway. The full uplift process can be visualized through the displacement sequences in Figure 12.

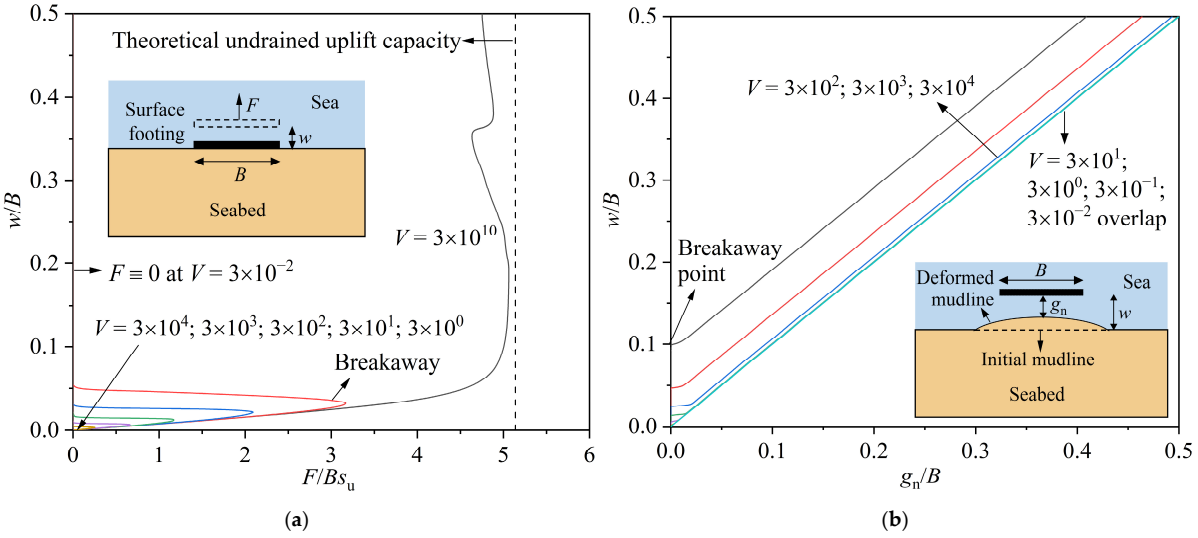


Figure 11. Performance of zero-thickness interface with Poiseuille tangential flow in simulating surface footing under uplift loading (adapted from Peng et al. [16]): (**a**) Dimensionless uplift force $F/(Bs_{u0})$–dimensionless uplift displacement w/B relationship; (**b**) Dimensionless gap opening width g_n/B–dimensionless uplift displacement w/B relationship.

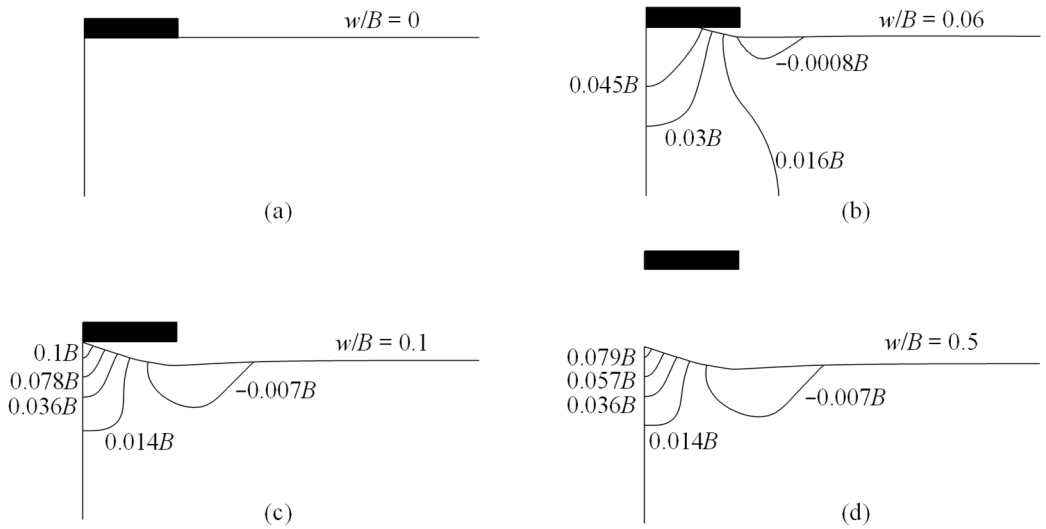


Figure 12. Illustration of the uplift process of a surface footing simulated using a zero-thickness interface with Poiseuille tangential flow (adapted from Peng et al. [16]): (**a**) $w/B = 0$; (**b**) $w/B = 0.06$; (**c**) $w/B = 0.1$; (**d**) $w/B = 0.5$.

Comparative analyses using the Darcy tangential flow model (Figure 13) demonstrate that while the general rate-dependent trends persist, the mechanical response is more gradual. In this case, the uplift force exhibits progressive softening rather than a distinct breakaway. The interfacial gap also develops at a significantly slower rate. This divergence is rooted in the sensitivity of the tangential flux (Q_t) to changes in the gap width (g_n). The Darcy tangential flux depends linearly on g_n in Equation (7), rendering it relatively insensitive to initial gap expansion. In contrast, the Poiseuille flux is proportional to the cube of g_n in Equation (6). As g_n increases, the cubic dependency triggers exponentially faster fluid infiltration and suction dissipation.

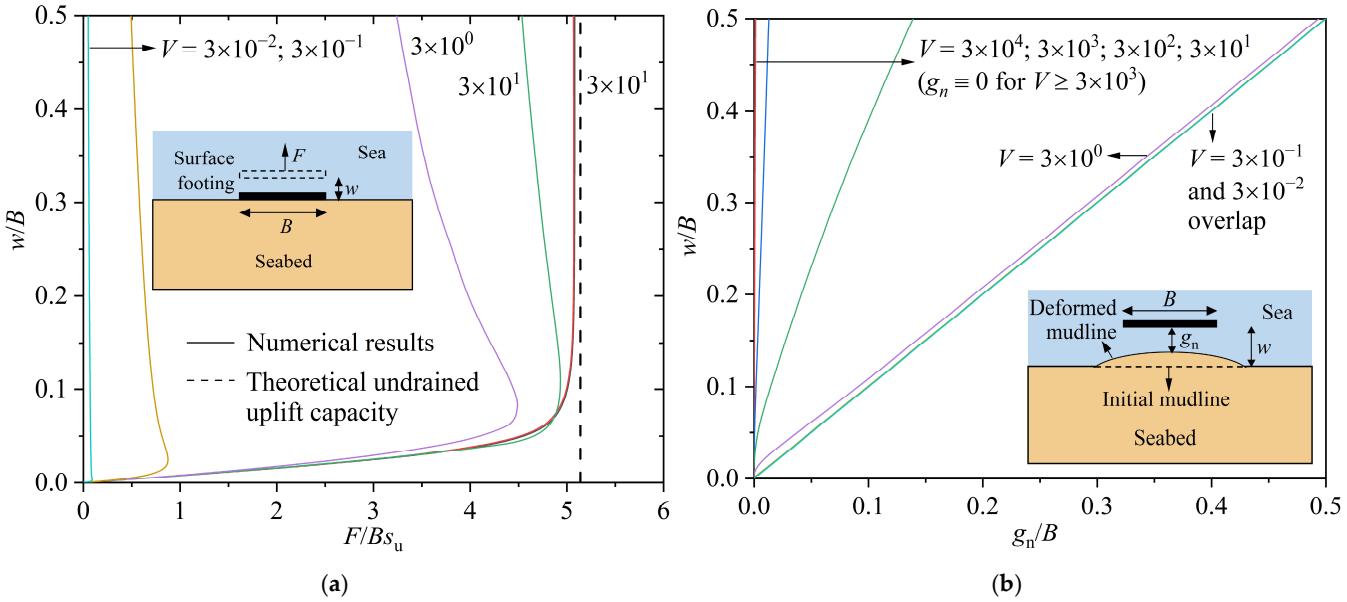


Figure 13. Performance of zero-thickness interface with Darcy tangential flow in simulating surface footing under uplift loading (adapted from Peng et al. [16]): (**a**) Dimensionless uplift force $F/(Bs_{u0})$–dimensionless uplift displacement w/B relationship; (**b**) Dimensionless gap opening width g_n/B–dimensionless uplift displacement w/B relationship.

Figure 14 presents the variation in peak uplift capacity with uplift velocity, derived from the results in Figures 11a and 13a, together with available centrifuge data [9,11,61] and predictions from conventional zero-suction and fully bonded interface models [62]. The H-M interface model reproduces the characteristic S-shaped increase in uplift capacity with logarithmic uplift velocity. In contrast, the conventional models predict rate-independent capacities and are applicable only at the fully drained and fully undrained limits.

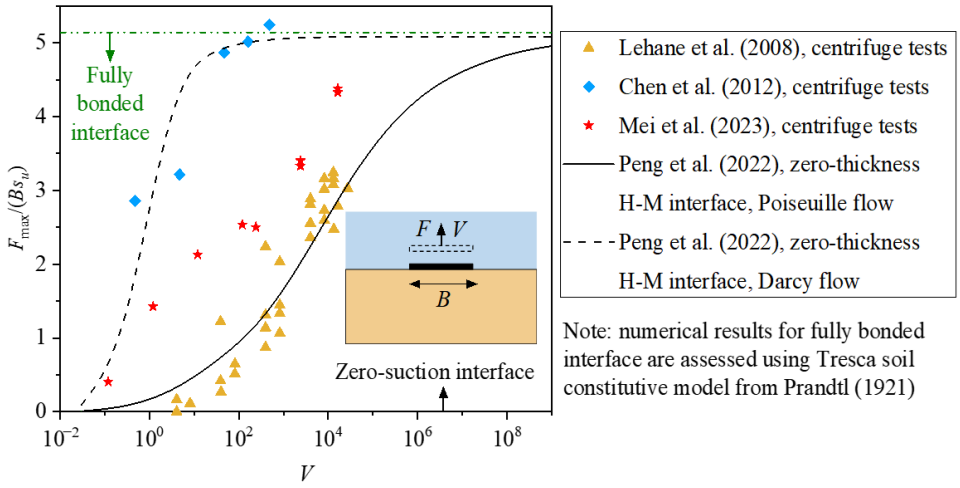


Figure 14. Uplift capacity–uplift rate relationships predicted using different interface models and comparison with centrifuge data (adapted from Peng et al. [16]).

This H-M zero-thickness interface provides direct and explicit control over the gap's physics, allowing both mild softening (Stage 2) and breakaway (Stage 3) to be simulated, thereby addressing one of the primary limitations of the thin-layer approach. Despite its predictive power and robust physical basis, the zero-thickness interface is generally more complex to implement than the thin-layer approach, typically necessitating the use of specialized in-house codes. The inclusion of frictional contact also makes the zero-thickness interface numerically less stable than its thin-layer counterpart. In addition, the conventional use of the leak-off formulation can introduce artificial numerical artifacts, such as the violation of local momentum conservation, as discussed by Peng et al. [26]. The calibration of the leak-off coefficients (c_1 and c_2) is also difficult and unconventional. To circumvent these issues, a modification was proposed by Peng et al. [26] to replace the leak-off equations with a direct pore pressure continuity condition $p_1 = p_g = p_2$. This eliminates the need for calibrating c_1 and c_2 while avoiding numerical artifacts.

4.2.2. Criterion for Breakaway

A comparison of the experimental data in Figure 2 with the numerical results in Figures 11a and 13b indicates that the transition from Stage 2 to Stage 3 (Figure 2) can be effectively modeled by switching the tangential flow regime from Darcy to Poiseuille mode. To formalize this concept, Peng et al. [15] proposed an empirical criterion to determine the timing of this transition:

$$\text{Breakaway happens when } d_r = d - \left(w - w_g\right) < \zeta d \tag{9}$$

where d is the total length of the skirt, d_r is the skirt length remaining buried in the seabed, w_g is the upward displacement of the mudline adjacent to the skirt, and ζ is a constant.

The physical interpretation of this criterion is schematically illustrated in Figure 15. As long as the skirt remains sufficiently embedded ($d_r/d > \zeta$), no direct open channel exists between the interface and the external seawater. In this regime, tangential water inflow

follows a Darcy-type transport mechanism, where the influx rate is linearly proportional to the gap width g_n. However, once the relative embedment reaches the critical threshold ($d_r/d = \zeta$), a preferential flow path is established, reflected by a sudden surge in the tangential influx rate.

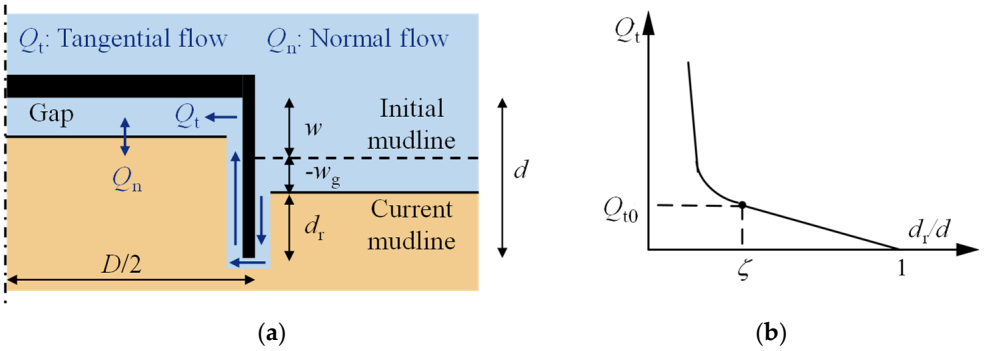


Figure 15. Illustration of breakaway criterion (adapted from Peng et al. [15]): (**a**) Schematic illustration; (**b**) Relationship between tangential flux Q_t and the dimensionless remaining skirt length in seabed d_r/d.

A salient feature of this formulation is its capacity to capture the rate-dependency of breakaway timing by accounting for the mudline displacement w_g. As shown in Figure 16, the mudline outside the foundation tends to move downward under undrained conditions due to pull-up of the soil plug inside the foundation, whereas the mudline moves slightly upward under drained conditions due to skirt friction. By incorporating the mudline displacement, the criterion effectively captures the experimental observation that higher uplift velocities trigger earlier breakaway.

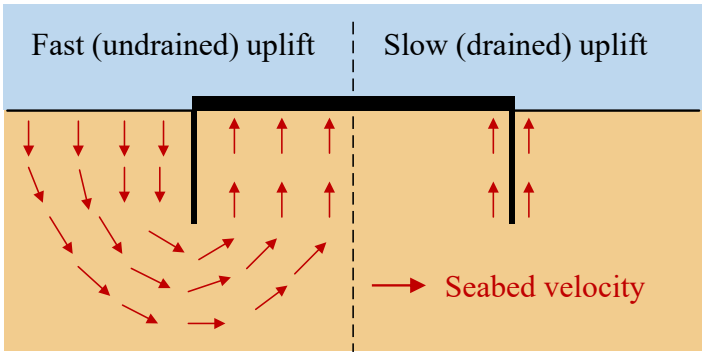


Figure 16. Illustration of the seabed deformation under uplift loading at different drainage states.

This breakaway criterion has been integrated into the H-M zero-thickness interface model to reproduce the centrifuge tests in Figure 2. The numerical breakaway timing demonstrates good quantitative agreement with the centrifuge data in Figure 17.

Note that the above is a preliminary attempt to understand and simulate the breakaway phenomenon. Specifically, the parameter ζ is an empirical constant defining the critical remaining skirt embedment required to prevent preferential water ingress and sudden suction loss. Although a constant value of ζ was shown to reasonably reproduce the breakaway timing observed in the centrifuge tests reported by Li [4], the universality of ζ remains unknown because of insufficient experimental data.

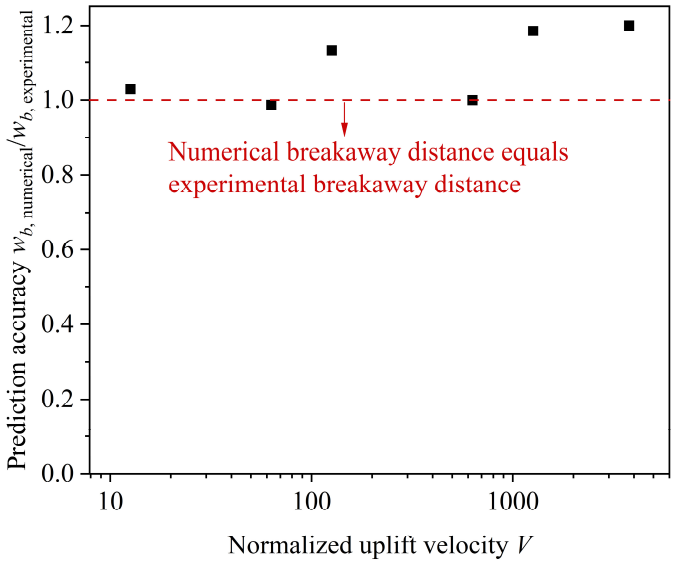


Figure 17. Performance of the proposed breakaway criterion in reproducing centrifuge tests (adapted from Peng et al. [15]).

4.2.3. Treatment of Cavitation

A primary limitation of the above zero-thickness interface is the omission of cavitation effects. This standard continuity Equation (8) assumes that changes in the interfacial gap volume are governed solely by pore-water influx from the surrounding seabed. In reality, cavitation may occur when the absolute gap water pressure falls to the local vapor pressure, particularly during rapid uplift in low-permeability soil, where water cannot infiltrate the opening gap sufficiently quickly. Under these conditions, part of the interfacial water changes phase from liquid to vapor, and the resulting volumetric expansion provides an additional mechanism for gap opening besides water influx. Cavitation therefore imposes an upper limit on the sustainable suction within the gap (e.g., the cavitation pressure). Because the H-M interface models described above assume a single-phase liquid and exclude this phase change contribution, they may predict unrealistically low gap water pressures and consequently overestimate the interfacial suction and uplift resistance.

To address this, Song et al. [63] undertook one of the first attempts to incorporate cavitation within the zero-thickness interface framework using a penalty H-M approach. This method introduces a threshold for the maximum allowable interfacial suction to simulate the onset of cavitation: $p_g \leq p_{cav}$, where p_{cav} is the cavitation pressure, estimated as $p_{cav} = -[p_{atm} + \gamma_w (h_w + y)]$, where p_{atm} is the atmospheric pressure, h_w is the water column depth above mudline, and y denotes the interface embedment depth. For a surface foundation or the underside of a suction caisson, $y = 0$. This maximum-suction constraint is integrated into the continuity Equation (8) via a penalty term:

$$-\nabla Q_t + v_{g1} + v_{g2} + \dot{g}_n + \underbrace{\lambda_w \langle p_{cav} - p_g \rangle}_{\text{Penalty term}} = 0 \tag{10}$$

where $< >$ is the Macaulay operator such that, for any value x, $< x > = 0$ if $x < 0$ and $< x > = x$ otherwise, and λ_w is a large penalty coefficient.

When the interfacial suction p_g remains above the threshold p_{cav}, the penalty term vanishes, and Equation (10) reverts to the standard H-M continuity Equation (8), consistent with non-cavitating conditions. Once p_g drops below p_{cav}, the penalty term becomes dominant in Equation (10). Because λ_w is several orders of magnitude larger than other

terms, Equation (10) approximately reduces to $\lambda_w (p_{cav} - p_g) = 0$, which is equivalent to $p_g = p_{cav}$, constraining the unphysically high suction to the defined cavitation limit.

While this approach limits suction magnitude, it fails to maintain mass conservation within the gap post-cavitation. The volumetric change associated with the phase transition from water to vapor is not linked to the gap opening rate. Instead, the post-cavitation mass conservation requirement degenerates into a simple pressure constraint $p_g = p_{cav}$, and the H-M interface degrades into a total stress interface with a constant interfacial tension.

A more physical treatment should replace the penalty term with a two-phase mass balance formulation. Unlike the penalty approach, which does not resolve the phase change process, the revised continuity equation should relate the change in gap volume to the net liquid flux and the volumetric contribution of evaporation or condensation. The liquid and vapor mass balances should be closed by equations of state of the vapor and a water-vapor phase equilibrium relation. If finite-rate non-equilibrium phase change is considered, an additional evaporation–condensation mass transfer law is required. The cavitation pressure would then emerge from the liquid–vapor state rather than being imposed numerically. This formulation would preserve H-M coupling and mass conservation while capturing the formation, growth, and collapse of the vapor cavity.

4.3. Comparison of H-M Interface Models

The H-M thin-layer and zero-thickness interface models differ primarily in their representation of the foundation-soil interface. The thin-layer model uses a finite-thickness porous continuum, providing a straightforward and numerically robust framework for combined *V-H-M* loading (vertical force, horizontal force, and overturning moment). However, gap opening is represented indirectly, and an abrupt breakaway cannot be reproduced. The zero-thickness model explicitly couples gap opening, contact, and fluid flow, allowing progressive softening and breakaway to be captured. Its greater complexity and lower numerical stability have thus far limited its application mainly to unidirectional uplift. Table 1 summarizes their principal features and applications.

Table 1. Comparison of H-M thin-layer and zero-thickness interface models.

Aspects	Thin-Layer H-M Interface	Zero-Thickness H-M Interface
Representation	Finite-thickness porous continuum	Discontinuity with zero geometric thickness
Mechanical formulation	Poroelasticity-based elastic or elastoplastic soil constitutive models	Normal and tangential contact laws governed by gap opening and sliding
Normal fluid exchange	Darcy seepage	Leak-off equations or Darcy seepage
Tangential fluid flow	Darcy seepage	Darcy-like flow for a quasi-closed gap or Poiseuille flow for an open gap
Gap opening	Represented indirectly by deformation of the interface layer	Represented explicitly by the normal gap width
Performance	Captures rate-dependent uplift resistance and mild post-peak softening but not abrupt breakaway or cavitation	Captures drainage-dependent resistance, mild softening, and abrupt breakaway. Cavitation can be incorporated through an appropriate phase change formulation, although the existing penalty-based treatment does not conserve mass after cavitation

Table 1. *Cont.*

Aspects	Thin-Layer H-M Interface	Zero-Thickness H-M Interface
Strengths	Greater numerical robustness; suitable for combined *V-H-M* multidirectional loading	More explicit representation of interface physics; particularly useful for mechanistic analysis of uplift behavior
Weaknesses	Gap opening is represented approximately; breakaway and cavitation are not explicitly captured	More complex implementation and lower numerical stability under shearing, rotation, and combined loading

5. Data-Enabled Techniques for H-M Interfacial Uplift Problems

Data-enabled modeling has recently attracted increasing attention in geotechnical and offshore engineering, providing new tools for constitutive modeling, inverse analysis, rapid prediction, and real-time state estimation. For uplift-related offshore foundation problems, early machine-learning applications mainly focused on capacity prediction. For example, Alavi et al. [64] used genetic-based modeling to predict the uplift capacity of suction caissons. Such studies demonstrate the potential of data-driven methods for rapid engineering prediction, but they generally treat uplift resistance as an input-output mapping and do not explicitly resolve the H-M coupled interface mechanisms, such as suction generation, drainage-dependent gap opening, breakaway, and interfacial fluid flow.

For interface behavior, Zhang et al. [65] developed a BiLSTM-based model for soil-structure interface modeling, showing that recurrent neural networks can reproduce complex path-dependent interface responses. However, existing interface-oriented machine-learning models mainly describe mechanical interface behavior and have not yet incorporated the coupled evolution of pore pressure, gap opening, and tensile fluid-mediated resistance under uplift loading. Therefore, their direct application to offshore foundation uplift remains limited.

Physics-informed neural networks (PINNs) provide another promising direction because they embed governing equations and boundary conditions into the learning process. The general PINN framework was established by Raissi et al. [66] for forward and inverse problems governed by nonlinear partial differential equations. In geotechnical engineering, Zhang et al. [67] applied PINNs to soil consolidation, demonstrating their ability to solve drainage-related deformation problems. More broadly, Amini et al. [68] used PINNs for inverse modeling of nonisothermal multiphase poromechanics, while Yang et al. [69] developed Bayesian PINNs for forward and inverse PDE problems with noisy data. These studies are relevant to H-M uplift problems because the governing mechanisms also involve coupled seepage and deformation. Nevertheless, most existing PINN applications treat the geomaterial as a continuum porous medium rather than a discontinuous foundation-soil interface with evolving gap opening, breakaway, and interfacial fluid flow. Extending PINNs to H-M zero-thickness or thin-layer interface formulations therefore remains an important open problem.

Surrogate modeling, optimization-based back-analysis, and Bayesian calibration are also highly relevant to H-M interfacial uplift problems. Parameters such as interface permeability, leak-off coefficients, breakaway criteria, and cavitation-related constants are difficult to determine directly from conventional element tests. Existing geotechnical studies have shown that intelligent optimization and updating methods can identify soil parameters and improve model predictions. For instance, Jin et al. [49] developed multi-objective optimization-based prediction updating during excavation. Although these studies are not focused on uplift interfaces, they provide useful methodological foundations for calibrating H-M interface models against centrifuge, model-scale, or field-monitoring

data. In future applications, surrogate models trained from high-fidelity H-M interface simulations could support rapid parametric design, while Bayesian updating could quantify uncertainty in interface parameters and uplift resistance.

Digital twins further extend data-enabled modeling from offline prediction to real-time monitoring and decision support. Semeraro et al. [70] reviewed the digital-twin paradigm and emphasized the integration of physical models, data, and feedback updating, while Thelen et al. [71] highlighted the roles of uncertainty quantification and optimization in digital-twin frameworks. For offshore foundations under uplift loading, a digital twin would require not only structural and operational monitoring, but also a physics-based H-M interface model capable of updating the evolving suction, gap state, drainage condition, and remaining uplift capacity using in situ measurements. At present, however, digital-twin applications rarely incorporate such H-M interfacial uplift mechanisms.

Overall, the available literature provides useful data-enabled tools, but a mature framework specifically addressing H-M coupled interfacial behavior under uplift loading has not yet been established. Integrating data-enabled techniques with the H-M interface models therefore represents an important frontier for future research.

6. Concluding Remarks and Future Perspectives

This paper provides a comprehensive synthesis of recent advancements in the hydro-mechanical (H-M) coupled uplift behavior of offshore foundations, tracing the progression from fundamental experimental insights to 1D analytical solutions and fully coupled 3D numerical simulations. The key conclusions and identified research frontiers are summarized as follows.

(1) Paradigm shift in uplift mechanism: from soil-structure to soil–fluid–structure interaction. A fundamental distinction exists between uplift and compressive loading. Experimental observations reveal a three-stage response comprising rapid mobilization, suction-controlled softening, and breakaway. Increased drainage accelerates gap opening and suction dissipation, thereby reducing uplift resistance. Unlike traditional compressive loading, uplift forces can induce detachment at the foundation-soil interface, leading to the progressive formation of a water-filled interfacial gap. This phenomenon effectively transforms the classical soil-structure interaction problem into the more complex framework of "soil–interfacial fluid–structure" interaction. Within this regime, the system's H-M response is primarily governed by the mass conservation and momentum balance of the interfacial fluid.

(2) Advancements in modeling and critical engineering implications. Moving beyond conventional total-stress interface models, specialized H-M interface models—ranging from easier-to-implement thin-layer interfaces to more physics-based zero-thickness interfaces—have been developed to more realistically simulate this transient coupled process. The 1D analytical model demonstrates that gap evolution is governed by the balance between interface opening and fluid influx. Thin-layer H-M models reproduce drainage-dependent resistance but represent gap opening indirectly and cannot capture abrupt breakaway, whereas zero-thickness models explicitly simulate gap evolution, fluid exchange, and breakaway but are more complex to implement. As offshore wind, subsea mining, and oil and gas operations migrate into deeper waters, floating systems are poised to become the dominant station-keeping solution. This makes accurate prediction of uplift capacity increasingly vital to safe and economical foundation design. This is particularly critical for shared anchoring systems designed for next-generation floating offshore wind turbines, where a single foundation must resist cumulative uplift loads from multiple turbines. The resulting forces are substantial, and the failure of a single anchor could trigger a

catastrophic, systemic collapse of the entire wind farm, underscoring the importance of adopting advanced H-M interface models.

(3) Current knowledge gaps and limitations. Despite significant progress in understanding H-M interfacial behavior and its numerical simulation, current knowledge is not yet sufficient to support high-fidelity replication of in situ conditions. The majority of existing research focuses on "wished-in-place" foundations under undrained, monotonic loading. However, the true engineering challenge lies in predicting the response to sustained operational uplift forces over a service life exceeding 20 years. These loading conditions can trigger interfacial gap formation and fundamentally alter the foundation's failure mechanism [12]. In addition, most existing H-M interface models have been developed for saturated clay and assessed primarily against monotonic centrifuge tests. Their applicability to other soil types and foundation geometries, cyclic and long-term loading, field-scale conditions, and cavitation remains insufficiently established.

(4) The research frontier: key challenges for future work. To bridge the gap between current knowledge and real-world conditions, future research must address the following critical areas:

- Multidirectional and eccentric uplift loading. The resultant external loads on offshore foundations are typically multidirectional and eccentric. This condition has primarily been investigated under fully undrained conditions for a fully closed interface. The corresponding H-M interfacial response under partial drainage remains poorly understood.
- Cyclic loading response. Hydrodynamic forces on offshore structures are inherently cyclic, due to the vertical motion of superstructures caused by ocean waves. Yet existing studies focus predominantly on monotonic uplift loading. Efforts are needed to reveal the H-M interfacial response under sustained cyclic loading.
- Suction-induced liquefaction in cohesionless seabeds. Most H-M interfacial research is confined to clays, leaving sandy and silty seabeds largely uncharacterized. The potential for seabed liquefaction triggered by interfacial suction [72–76], and its influence on ultimate uplift capacity, warrants thorough investigation.
- Long-term evolution and rheology. In situ foundations endure force-controlled loading across decades, yet most studies employ constant-rate displacement under monotonic conditions. A complete picture requires accounting for the combined effects of sustained, cyclic, and multidirectional loading. Furthermore, the influence of soil's rheological properties on long-term interface integrity, analogous to studies on pipelines under compressive loading [77], represents a vital new research direction.
- Broader database and engineering application. Existing experimental and numerical studies have focused primarily on clay seabeds under monotonic uplift. Future work should establish broader laboratory and field datasets across different soils, foundation geometries, and loading conditions to support the development and assessment of numerical models. These advances should be translated into practical guidance for model selection, parameter calibration, and foundation design, allowing interface suction to be accounted for reliably in more cost-effective offshore foundation designs.
- Embracing the emerging data-enabled techniques. Physics-informed machine learning, data-driven constitutive models, reduced-order models, and digital twins show considerable promise for soil-structure interaction modeling. However, existing applications [65,67] largely focus on total-stress interface mechanics, parameter identification, and simplified interaction surrogates, without addressing transient H-M interfacial processes. Future research should integrate these techniques with H-M interface formulations and experimental or field measurements to enable efficient long-term prediction and real-time identification of interface states.

Author Contributions: Conceptualization, F.G., M.P.; data analyses, M.P., S.M.; writing—original draft, M.P.; review and editing, F.G., M.P., S.M., J.C. All authors have read and agreed to the published version of the manuscript.

Funding: This work was funded by the National Natural Science Foundation of China (Grant No. 12061160463) and the Research Grants Council (RGC) of Hong Kong Joint Research Scheme (Grant No. N_PolyU534/20).

Data Availability Statement: The data presented in this study are available upon request from the corresponding author.

Conflicts of Interest: The authors declare no conflicts of interest.

Notations

V, v	Dimensionless and physical uplift velocity
D, d	Diameter and skirt length of skirted foundation
c_v	Coefficient of consolidation
$\mathbf{v}_w$	Seepage velocity of pore water in seabed
K	Permeability of soil
K_g	Tangential permeability of interface for Darcy tangential flow
γ_w	Unit weight of water
p, p'	Excess pore water pressure and soil mean effective stress
q	A uniform tension or compression
z	Vertical elevation
h_1, h_2	Heights of Object 1 and Object 2
t, T, t_1	Physical time, dimensionless time, dimensionless time for Object 1
E, ν	Young's modulus and Poisson's ratio
g_n, g_t	Gap opening width, gap tangential sliding distance
$\boldsymbol{\sigma}'$, $\mathbf{b}$	Effective stress tensor, body force vector
ε_v	Volumetric strain
e, e_0	Void ratio, void ratio at $p' = 1$
κ	Bulk modulus of porous elastic material
$\mathbf{s}$, $\boldsymbol{\varepsilon}_d$	Deviatoric stress tensor, deviatoric strain tensor
k_n, k_t, υ	Interface normal, tangential stiffness, and frictional coefficient
p_1, p_2, p_g	Excess water pressure at contacting surfaces and inside interface
v_{g1}, v_{g2}	Water exchange rate at contacting surfaces
c_1, c_2	Leak-off coefficients at contacting surfaces
Q_n	Normal flux rate into the interface
Q_t, Q_{t0}	Tangential flux rate inside interface, critical flux rate at breakaway
μ	Dynamic viscosity of water
d_r	Length of skirt remaining buried in seabed
w, w_g	Upward displacement of foundation and seabed
ζ	A constant factor controlling breakaway timing
p_{cav}, p_{atm}	Cavitation pressure and atmospheric pressure
h_w, y	Water column depth above foundation, and foundation embedment
λ_w	Penalty coefficient associated with the cavitation term
F, s_{u0}	Uplift force and the soil undrained shear strength beneath foundation
A, B	Cross-sectional area and width of the foundation
v_n, v_t	Normal and tangential flow velocity of interfacial fluid

References

1. GWEC. *Global Offshore Wind Report 2025*; GWEC: Lisbon, Portugal, 2025. Available online: https://26973329.fs1.hubspotusercontent-eu1.net/hubfs/26973329/2.%20Reports/Global%20Wind%20Report/GWEC%20Global%20Wind%20Report%202025.pdf (accessed on 27 June 2026).

2. Amaechi, C.V.; Reda, A.; Butler, H.O.; Ja'e, I.A.; An, C. Review on fixed and floating offshore structures. Part I: Types of platforms with some applications. *J. Mar. Sci. Eng.* **2022**, *10*, 1074. [CrossRef]
3. Sergiienko, N.; Da Silva, L.; Bachynski-Polić, E.; Cazzolato, B.; Arjomandi, M.; Ding, B. Review of scaling laws applied to floating offshore wind turbines. *Renew. Sustain. Energy Rev.* **2022**, *162*, 112477. [CrossRef]
4. Li, X. The Uplift of Offshore Shallow Foundations. Ph.D. Thesis, The University of Western Australia, Crawley, WA, Australia, 2015.
5. Acosta-Martinez, H.; Gourvenec, S.; Randolph, M. Centrifuge study of capacity of a skirted foundation under eccentric transient and sustained uplift. *Geotechnique* **2012**, *62*, 317–328. [CrossRef]
6. Gourvenec, S.; Acosta-Martinez, H.; Randolph, M. Experimental study of uplift resistance of shallow skirted foundations in clay under transient and sustained concentric loading. *Geotechnique* **2009**, *59*, 525–537. [CrossRef]
7. Purwana, O.; Leung, C.; Chow, Y.; Foo, K. Influence of base suction on extraction of jack-up spudcans. *Geotechnique* **2005**, *55*, 741–753. [CrossRef]
8. Mana, D.S.; Gourvenec, S.; Randolph, M.F. Experimental investigation of reverse end bearing of offshore shallow foundations. *Can. Geotech. J.* **2013**, *50*, 1022–1033. [CrossRef]
9. Chen, R.; Gaudin, C.; Cassidy, M. Investigation of the vertical uplift capacity of deep water mudmats in clay. *Can. Geotech. J.* **2012**, *49*, 853–865. [CrossRef]
10. Tian, Y.; Ren, J.; Zhou, T.; Peng, M.; Cassidy, M.J. Coupled hydro-mechanical interfaces to enable uplift modelling in offshore engineering. *Ocean Eng.* **2022**, *245*, 110570. [CrossRef]
11. Mei, S.; Tian, Y.; Cassidy, M.J.; O'Loughlin, C. Experimental investigation of rate effects on the uplift response of surface and skirted circular shallow foundations. *J. Geotech. Geoenviron. Eng.* **2025**, *151*, 04024149. [CrossRef]
12. Han, C.; Wang, D.; Gaudin, C.; O'Loughlin, C.; Cassidy, M. Behaviour of vertically loaded plate anchors under sustained uplift. *Geotechnique* **2016**, *66*, 681–693. [CrossRef]
13. Hu, C.; Gao, F.-P. Elasto-plasticity and pore-pressure coupled analysis on the pullout behaviors of a plate anchor. *Theor. Appl. Mech. Lett.* **2015**, *5*, 89–92.
14. Mana, D.S.; Gourvenec, S.M.; Randolph, M.F.; Hossain, M.S. Failure mechanisms of skirted foundations in uplift and compression. *Int. J. Phys. Model. Geotech.* **2012**, *12*, 47–62. [CrossRef]
15. Peng, M.; Tian, Y.; Gaudin, C. Investigations into the Uplift of Skirted Foundations on Clay at Varying Rates. *J. Geotech. Geoenviron. Eng.* **2024**, *150*, 04023137. [CrossRef]
16. Peng, M.; Tian, Y.; Gaudin, C.; Zhang, L.; Sheng, D. Application of a coupled hydro-mechanical interface model in simulating uplifting problems. *Int. J. Numer. Anal. Methods Geomech.* **2022**, *46*, 3256–3280.
17. Peng, M.; Yin, Z.-Y.; Zhou, Z. Numerical investigations into the influence of drainage on the uplift behaviour of plate anchors in clay. *Comput. Geotech.* **2025**, *181*, 107128. [CrossRef]
18. Zhang, G.; Zhang, J. State of the art: Mechanical behavior of soil-structure interface. *Prog. Nat. Sci.* **2009**, *19*, 1187–1196.
19. Wang, X.; Zeng, X.; Li, J.; Yang, X.; Wang, H. A review on recent advancements of substructures for offshore wind turbines. *Energy Convers. Manag.* **2018**, *158*, 103–119. [CrossRef]
20. Oh, K.-Y.; Nam, W.; Ryu, M.S.; Kim, J.-Y.; Epureanu, B.I. A review of foundations of offshore wind energy convertors: Current status and future perspectives. *Renew. Sustain. Energy Rev.* **2018**, *88*, 16–36. [CrossRef]
21. Dhadse, G.D.; Ramtekkar, G.; Bhatt, G. Finite Element Modeling of Soil Structure Interaction System with Interface: A Review. *Arch. Comput. Methods Eng.* **2021**, *28*, 3415–3432.
22. Finnie, I.M.S.; Randolph, M. Punch-through and liquefaction induced failure of shallow foundations on calcareous sediments. In Proceedings of the 7th International Conference on the Behaviour of Offshore Structures, Pergamon, MA, USA, 12–15 July 1994; pp. 217–230.
23. Acosta-Martinez, H.E.; Gourvenec, S.M.; Randolph, M.F. An experimental investigation of a shallow skirted foundation under compression and tension. *Soils Found.* **2008**, *48*, 247–254. [CrossRef]
24. Acosta-Martinez, H.E.; Gourvenec, S.M.; Randolph, M.F. Effect of gapping on the transient and sustained uplift capacity of a shallow skirted foundation in clay. *Soils Found.* **2010**, *50*, 725–735. [CrossRef]
25. Mei, S.; Tian, Y.; Cassidy, M.J.; O'Loughlin, C. Experimental Study on the Behavior of Bucket Foundations under Sustained Uplift Loading. *J. Geotech. Geoenviron. Eng.* **2026**, *152*, 04026018. [CrossRef]
26. Peng, M.; Fang, H.; Tian, Y. An HM contact model to simulate soil-structure interactions under tension in offshore environments. *Comput. Geotech.* **2025**, *180*, 107025.
27. Song, Z.H.; Hu, Y.X.; Randolph, M.F. Numerical simulation of vertical pullout of plate anchors in clay. *J. Geotech. Geoenviron. Eng.* **2008**, *134*, 866–875. [CrossRef]
28. Rowe, R.K.; Davis, E.H. The Behavior of Anchor Plates in Clay. *Geotechnique* **1982**, *32*, 9–23.
29. Merifield, R.; Lyamin, A.; Sloan, S.; Yu, H. Three-dimensional lower bound solutions for stability of plate anchors in clay. *J. Geotech. Geoenviron. Eng.* **2003**, *129*, 243–253. [CrossRef]

30. Yu, L.; Liu, J.; Kong, X.J.; Hu, Y. Numerical study on plate anchor stability in clay. *Geotechnique* **2011**, *61*, 235–246. [CrossRef]
31. Wu, X.; Chow, Y.K.; Leung, C.F. Behavior of drag anchor under uni-directional loading and combined loading. *Ocean Eng.* **2017**, *129*, 149–159. [CrossRef]
32. Wei, W.; Tang, H. Analysis of the ultimate uplift resistance and progressive failure process of strip plate anchors in marine sensitive clays: A FE analysis based on micropolar continuum theory. *Can. Geotech. J.* **2025**, *62*, 1–23.
33. Wang, D.; Hu, Y.X.; Randolph, M.F. Three-Dimensional Large Deformation Finite-Element Analysis of Plate Anchors in Uniform Clay. *J. Geotech. Geoenviron. Eng.* **2010**, *136*, 355–365.
34. Gens, A.; Carol, I.; Alonso, E. A constitutive model for rock joints formulation and numerical implementation. *Comput. Geotech.* **1990**, *9*, 3–20. [CrossRef]
35. Maitra, S.; White, D.; Chatterjee, S.; Choudhury, D. Numerical modelling of seepage and tension beneath plate anchors. *Comput. Geotech.* **2019**, *108*, 131–142. [CrossRef]
36. Mana, D.S.K.; Gourvenec, S.; Randolph, M.F. Numerical modelling of seepage beneath skirted foundations subjected to vertical uplift. *Comput. Geotech.* **2014**, *55*, 150–157. [CrossRef]
37. Desai, C.; Zaman, M.; Lightner, J.; Siriwardane, H. Thin-layer element for interfaces and joints. *Int. J. Numer. Anal. Methods Geomech.* **1984**, *8*, 19–43.
38. Beer, G. An isoparametric joint/interface element for finite element analysis. *Int. J. Numer. Methods Eng.* **1985**, *21*, 585–600. [CrossRef]
39. Biot, M.A. General theory of three-dimensional consolidation. *J. Appl. Phys.* **1941**, *12*, 155–164. [CrossRef]
40. Qi, W.; Shi, Y.; Gao, F. Uplift soil resistance to a shallowly-buried pipeline in the sandy seabed under waves: Poro-elastoplastic modeling. *Appl. Ocean Res.* **2020**, *95*, 102024.
41. Kwa, K.; White, D. Numerical modelling of plate anchors under sustained load: The enhancement of capacity from consolidation. *Comput. Geotech.* **2023**, *158*, 105367. [CrossRef]
42. Qi, W.; Shi, Y.; Gao, F. Poro-elastoplastic modelling of uplift resistance of shallowly-buried pipelines. In *International Conference on Offshore Mechanics and Arctic Engineering*; American Society of Mechanical Engineers: New York, NY, USA, 2017.
43. Wang, D.; Hu, Y.; Randolph, M.F. Effect of loading rate on the uplift capacity of plate anchors. In *The Eighteenth International Offshore and Polar Engineering Conference*; OnePetro: Richardson, TX, USA, 2008.
44. Small, J.; Thorne, C.; Ta, L. Effect of pore pressure dissipation on the behaviour of anchors in clay. In *The Eighth International Offshore and Polar Engineering Conference*; OnePetro: Richardson, TX, USA, 1998.
45. Schofield, A.N.; Wroth, P. *Critical State Soil Mechanics*; McGraw-Hill: London, UK, 1968; Volume 310.
46. Gens, A.; Potts, D. Critical state models in computational geomechanics. *Eng. Comput.* **1988**, *5*, 178–197. [CrossRef]
47. Peng, M.; Yin, Z.-Y. Numerical investigations into the drainage effects on the behaviors of plate anchors under unidirectional and combined loadings. *Comput. Geotech.* **2025**, *188*, 107624. [CrossRef]
48. Jin, Y.F.; Yin, Z.Y.; Shen, S.L.; Hicher, P.Y. Selection of sand models and identification of parameters using an enhanced genetic algorithm. *Int. J. Numer. Anal. Methods Geomech.* **2016**, *40*, 1219–1240.
49. Jin, Y.-F.; Yin, Z.-Y.; Zhou, W.-H.; Huang, H.-W. Multi-objective optimization-based updating of predictions during excavation. *Eng. Appl. Artif. Intell.* **2019**, *78*, 102–123.
50. Jin, Y.F.; Yin, Z.Y. Enhancement of backtracking search algorithm for identifying soil parameters. *Int. J. Numer. Anal. Methods Geomech.* **2020**, *44*, 1239–1261. [CrossRef]
51. Ng, K.; Small, J. Behavior of joints and interfaces subjected to water pressure. *Comput. Geotech.* **1997**, *20*, 71–93. [CrossRef]
52. Cerfontaine, B.; Dieudonné, A.-C.; Radu, J.-P.; Collin, F.; Charlier, R. 3D zero-thickness coupled interface finite element: Formulation and application. *Comput. Geotech.* **2015**, *69*, 124–140. [CrossRef]
53. Segura, J.; Carol, I. On zero-thickness interface elements for diffusion problems. *Int. J. Numer. Anal. Methods Geomech.* **2004**, *28*, 947–962.
54. Segura, J.; Carol, I. Coupled HM analysis using zero-thickness interface elements with double nodes—Part II: Verification and application. *Int. J. Numer. Anal. Methods Geomech.* **2008**, *32*, 2103–2123.
55. Song, C.; Tang, X.; Uzuoka, R.; Luan, Y.; Wang, K.; Li, M. Suction caisson uplift behavior in multilayered sand under varying drainage conditions. *Ocean Eng.* **2025**, *332*, 121361. [CrossRef]
56. Snow, D. A Parallel Plate Model of Fractured Permeable Media. Ph.D. Thesis, University of California, Berkeley, CA, USA, 1965.
57. Goodman, R.E.; Taylor, R.L.; Brekke, T.L. A model for the mechanics of jointed rock. *J. Soil. Mech. Found. Div.* **1968**, *94*, 637–659. [CrossRef]
58. Day, R.A.; Potts, D.M. Zero Thickness Interface Elements—Numerical Stability and Application. *Int. J. Numer. Anal. Methods Geomech.* **1994**, *18*, 689–708. [CrossRef]
59. Lai, Y.; Chen, C.; Zhu, B.; Dai, J.-l.; Kong, D.-q. Numerical modelling on effect of loading rate on uplift behavior of suction caissons. *Ocean Eng.* **2022**, *260*, 112013. [CrossRef]

60. Mei, S.; Tian, Y.; Cassidy, M.J. Numerical modelling of the uplift process and breakaway of circular surface footings. *Comput. Geotech.* **2025**, *179*, 106952.
61. Lehane, B.M.; Gaudin, C.; Richards, D.J.; Rattley, M.J. Rate effects on the vertical uplift capacity of footings founded in clay. *Geotechnique* **2008**, *58*, 13–21. [CrossRef]
62. Prandtl, L. Hauptaufsätze: Über die eindringungsfestigkeit (härte) plastischer baustoffe und die festigkeit von schneiden. *Z. Angw. Math. Mech.* **1921**, *1*. [CrossRef]
63. Song, C.; Tang, X.; Uzuoka, R. Numerical analysis of the effect of cavitation on tensile capacity during suction caisson uplift. *Comput. Geotech.* **2026**, *190*, 107733.
64. Alavi, A.H.; Aminian, P.; Gandomi, A.H.; Esmaeili, M.A. Genetic-based modeling of uplift capacity of suction caissons. *Expert. Syst. Appl.* **2011**, *38*, 12608–12618. [CrossRef]
65. Zhang, P.; Yang, Y.; Yin, Z.-Y. BiLSTM-based soil-structure interface modeling. *Int. J. Geomech.* **2021**, *21*, 04021096.
66. Raissi, M.; Perdikaris, P.; Karniadakis, G.E. Physics-informed neural networks: A deep learning framework for solving forward and inverse problems involving nonlinear partial differential equations. *J. Comput. Phys.* **2019**, *378*, 686–707. [CrossRef]
67. Zhang, S.; Lan, P.; Li, H.-C.; Tong, C.-X.; Sheng, D. Physics-informed neural networks for consolidation of soils. *Eng. Comput.* **2022**, *39*, 2845–2865. [CrossRef]
68. Amini, D.; Haghighat, E.; Juanes, R. Inverse modeling of nonisothermal multiphase poromechanics using physics-informed neural networks. *J. Comput. Phys.* **2023**, *490*, 112323. [CrossRef]
69. Yang, L.; Meng, X.; Karniadakis, G.E. B-PINNs: Bayesian physics-informed neural networks for forward and inverse PDE problems with noisy data. *J. Comput. Phys.* **2021**, *425*, 109913.
70. Semeraro, C.; Lezoche, M.; Panetto, H.; Dassisti, M. Digital twin paradigm: A systematic literature review. *Comput. Ind.* **2021**, *130*, 103469. [CrossRef]
71. Thelen, A.; Zhang, X.; Fink, O.; Lu, Y.; Ghosh, S.; Youn, B.D.; Todd, M.D.; Mahadevan, S.; Hu, C.; Hu, Z. A comprehensive review of digital twin—Part 2: Roles of uncertainty quantification and optimization, a battery digital twin, and perspectives. *Struct. Multidiscip. Optim.* **2023**, *66*, 1.
72. Qi, W.; Gao, F. Wave induced instantaneously-liquefied soil depth in a non-cohesive seabed. *Ocean Eng.* **2018**, *153*, 412–423.
73. Li, C.; Yu, J.; Gao, F. Phase-lag effect on the instantaneously-liquefied seabed depth under progressive waves: Explicit approximations. *Appl. Ocean Res.* **2024**, *147*, 103965.
74. Yamamuro, J.A.; Lade, P.V. Static liquefaction of very loose sands. *Can. Geotech. J.* **1997**, *34*, 905–917. [CrossRef]
75. Ng, C.W.; Crous, P.A.; Zhang, M.; Shakeel, M. Static liquefaction mechanisms in loose sand fill slopes. *Comput. Geotech.* **2022**, *141*, 104525. [CrossRef]
76. Kramer, S.L.; Seed, H.B. Initiation of soil liquefaction under static loading conditions. *J. Geotech. Eng.* **1988**, *114*, 412–430. [CrossRef]
77. Cheng, J.; Li, J.; Gao, F.; Yin, Z.-Y. Long-term settlement of deepsea pipelines on a soft clayey seabed: Poro-elasto-viscoplastic modeling. *Ocean Eng.* **2025**, *332*, 121414.

Disclaimer/Publisher's Note: The statements, opinions and data contained in all publications are solely those of the individual author(s) and contributor(s) and not of MDPI and/or the editor(s). MDPI and/or the editor(s) disclaim responsibility for any injury to people or property resulting from any ideas, methods, instructions or products referred to in the content.